
Article:

Maunder, A., Chan, H. orcid.org/0000-0002-5382-2097, Hughes, P.J.C. orcid.org/0000-0002-7979-5840 et al. (7 more authors) (2021) MR properties of 19F C3F8 gas in the lungs of healthy volunteers: T2* and apparent diffusion coefficient at 1.5T and T2* at 3T. Magnetic Resonance in Medicine, 85 (3). pp. 1561-1570. ISSN 0740-3194

https://doi.org/10.1002/mrm.28511

Received: 30 May 2020 | Revised: 8 August 2020 | Accepted: 17 August 2020

DOI: 10.1002/mrm.28511

NOTE

Magnetic Resonance in Medicine

MR properties of ^{19}F C_3F_8 gas in the lungs of healthy volunteers: T_2^* and apparent diffusion coefficient at 1.5T and T_2^* at 3T

Adam Maunder[1] | Ho-Fung Chan[1] | Paul J. C. Hughes[1] | Guillhem Collier[1] | Graham Norquay[1] | Oliver Rodgers[1] | Peter Thelwall[2] | Fraser Robb[1,3] | Madhwesha Rao[1] | Jim M. Wild[1]

[1]POLARIS, Imaging Group, Department of IICD, University of Sheffield, Sheffield, United Kingdom

[2]Newcastle Magnetic Resonance Centre, Newcastle University, Newcastle upon Tyne, United Kingdom

[3]GE Healthcare, Aurora, Ohio, USA

Correspondence
Jim M. Wild, POLARIS, Imaging Group, Department of Infection, Immunity & Cardiovascular Disease, University of Sheffield, C Floor, Royal Hallamshire Hospital, Sheffield, S10 2JF, United Kingdom.
Email: j.m.wild@sheffield.ac.uk

Funding information
National Institute for Health Research (NIHR-RP-R3-12-027), the Medical Research Council (MR/M008894/1), the National Sciences and Engineering Research Council of Canada (NSERC), an investigator-led research grant from GE Healthcare, LIFT MRC project MR/N018915/1, and a research grant from GlaxoSmithKline (BIDS3000032592).

Purpose: To measure the transverse relaxation time (T_2^*) and apparent diffusion coefficient (ADC) of ^{19}F-C_3F_8 gas in vivo in human lungs at 1.5T and 3T, and to determine the representative distribution of values of these parameters in a cohort of healthy volunteers.

Methods: Mapping of ADC at lung inflation levels of functional residual capacity (FRC) and total lung capacity (TLC) was performed with inhaled ^{19}F-C_3F_8 (eight subjects) and ^{129}Xe (six subjects) at 1.5T. T_2^* mapping with ^{19}F-C_3F_8 was performed at 1.5T (at FRC and TLC) for 8 subjects and at 3T (at TLC for seven subjects).

Results: At both FRC and TLC, the ^{19}F-C_3F_8 ADC was smaller than the free diffusion coefficient demonstrating airway microstructural diffusion restriction. From FRC to TLC, the mean ADC significantly increased from 1.56 mm^2/s to 1.83 mm^2/s ($P = .0017$) for ^{19}F-C_3F_8, and from 2.49 mm^2/s to 3.38 mm^2/s ($P = .0015$) for ^{129}Xe. The posterior-to-anterior gradient in ADC for FRC versus TLC in the superior half of the lungs was measured as 0.0308 mm^2/s per cm versus 0.0168 mm^2/s per cm for ^{19}F-C_3F_8 and 0.0871 mm^2/s per cm versus 0.0326 mm^2/s per cm for ^{129}Xe. A consistent distribution of ^{19}F-C_3F_8 T_2^* values was observed in the lungs, with low values observed near the diaphragm and large pulmonary vessels. The mean T_2^* across volunteers was 4.48 ms at FRC and 5.33 ms at TLC for 1.5T, and 3.78 ms at TLC for 3T.

Conclusion: In this feasibility study, values of physiologically relevant parameters of lung microstructure measurable by MRI (T_2^*, and ADC) were established for C_3F_8 in vivo lung imaging in healthy volunteers.

1 | INTRODUCTION

Currently, lung imaging with fluorinated gases (SF_6, C_2F_6, C_3F_8, C_4F_8[1]) MRI is not as well-characterized as hyperpolarized (HP) gas MRI, with a relative paucity in the literature. For example, there have already been numerous longitudinal and clinical studies performed with ^{3}He and ^{129}Xe gases.[2-4] In addition, typical values of MR measurable parameters for gas phase ^{3}He

and ^{129}Xe have been characterized in vivo, such as T_2^*,[5-7] T_1,[8] T_2,[9] and the apparent diffusion coefficient (ADC).[10-13] These values have been used to optimize pulse sequence design for improved ventilation image quality,[14-16] and also to inform diffusion-weighted imaging (DWI) acquisition strategies for quantitative microstructural imaging with ^{3}He and ^{129}Xe.[11,12,17]

The inherently low MR signal and short T_2^* of fluorinated gases results in lower signal-to-noise ratio (SNR) and necessitates lower image resolution when compared with HP gas imaging.[18] Recently, there have been advances in sequence optimization for fluorinated gas imaging using ultrashort echo time and steady-state free precession methods.[19,20] However, to date, there has only been preliminary investigation on whether fluorinated gas imaging can be used routinely to provide suitably robust quantitative measures of lung microstructure and function.[21-23]

1.1 | Transverse relaxation—T_2^*

The T_2^* relaxation parameter has been shown to depend on physiological changes in different tissues/organs with ^{1}H MRI,[24,25] and is, therefore, an important parameter for quantitative imaging. For C_3F_8 in phantoms, T_1, T_2, and T_2^* is approximately 6-8 ms when diluted in nearly 100% O_2 and approximately 18–20 ms for undiluted (100%) C_3F_8 at 95.2 kPa. In contrast, for ^{129}Xe and ^{3}He the T_1 reduces from hours to less than 30 s when mixed with O_2[28,29] in the lungs, whereas the T_2 is lower than 3 s. When measured in human lungs T_2^* is 28 ms and 14 ms at 1.5T and 3 T for ^{3}He[30,31], respectively, and 52 ms and 24 ms at 1.5 T and 3T for ^{129}Xe,[6] respectively. The T_2^* of HP gases has also been shown to change with lung inflation level and decreases at distinct physical susceptibility interfaces, such as around the major blood vessels and at the diaphragm,[6] though correlation with disease pathologies has not yet been studied. The T_2^* for C_3F_8 (measured through nonlocalized lung spectroscopy) has been shown to be sensitive to modulation of tissue magnetic susceptibility,[23] thus the T_2^* may also be a sensitive marker of lung microstructure variation.

1.2 | Apparent diffusion coefficient

In lung imaging with HP ^{3}He and ^{129}Xe, DWI is routinely used to probe the lung microstructure using the measurement of ADC and theoretical models of multiple b-value HP gas DWI.[10,32-34] The measured ADC is sensitive to changes in alveolar dimensions with diseases, such as emphysema,[11] idiopathic pulmonary fibrosis,[35,36] and chronic obstructive pulmonary disease.[37,38] Furthermore, even relatively small ADC changes related to lung inflation level,[39,40] age,[41] and physiological distribution within the lungs[42] are observable.

ADC measurements with fluorinated gases have been performed in rats with C_2F_6[43,44] and SF_6,[45] demonstrating that there is restricted diffusion and that the ADC is larger in emphysematous lungs. In contrast to measurements made in excised lungs with 100% C_2F_6[46] and C_3F_8,[47] performing in vivo ADC measurements with 79% C_3F_8 + 21% O_2 will accurately provide a normative range of values and distribution across healthy subjects. Furthermore, such a study will establish the feasibility of performing in vivo C_3F_8 ADC studies with the constraints imposed by the sensitivity of a thoracic radiofrequency (RF) coil, breath-hold limitations on image acquisition time, and the variability of gas concentration through voluntary continual breathing rather than controlled pumping.

1.3 | Overview

Determining the relative sensitivity and achievable quality of DWI with C_3F_8 in relation to ^{129}Xe was one aim of this study. Furthermore, the value and distribution of T_2^* in vivo is also unknown. Therefore, in this study theT_2^* and ADC with ^{19}F imaging of 79% C_3F_8 + 21% O_2 was investigated in the lungs of healthy volunteers. In the same eight volunteers, T_2^* mapping was carried out and the change from TLC to FRC was evaluated at 1.5T. In addition, T_2^* mapping at TLC was performed at 3T in seven of the volunteers to evaluate the field strength dependence of T_2^*. To determine the sensitivity of C_3F_8 ADC to changes in lung microstructural length scales, the differences obtained at FRC or TLC, and the regional distribution within the lungs, was investigated in eight healthy volunteers. ADC mapping with ^{129}Xe was carried out in six of the volunteers as a means of comparison with the equivalent established and higher SNR HP gas techniques.

2 | METHODS

2.1 | Overview

In total, eight subjects, seven male and one female (S1-S8, aged 29 ± 4 years), were imaged following informed consent. All in vivo MRI experiments were performed under the approval of the UK National Research Ethics Committee and the local National Health Service research office. The clinical grade 79% C_3F_8/21% O_2 gas mixture (BOC Special Products, Guildford, UK) was inhaled from a 25-L reservoir bag via a mouthpiece and three-way valve and mouthpiece (Hans Rudolf, Shawnee, KS). Hyperpolarization (~30%-40%) of 86% enriched ^{129}Xe gas was performed in house using the spin-exchange optical pumping method[48] under the corresponding author's UK MHRA manufacturing regulatory license.

2.2 | Radiofrequency coils

^{1}H and ^{19}F imaging was performed at 3T (Philips Ingenia; Philips, Andover, MA) using an elliptical transmit/receive quadrature birdcage coil (RAPID Biomedical, Rimpar, Germany). Experiments at 1.5T (GE HDx; GE Medical Systems, Milwaukee, WI) with ^{19}F were performed with an in-house constructed transceiver array,[49,50] which improves the average SNR by a factor of approximately 5 throughout the lung region when compared with a single transceiver vest coil. ^{129}Xe imaging at 1.5T was performed with a flexible transceiver vest coil (Clinical MR Solutions [CMRS], Brookfield, WI).

2.3 | Imaging

Table 1 lists the various imaging acquisition parameters for both C_3F_8 and ^{129}Xe scanning. In vivo ^{19}F-C_3F_8 T_2^* measurements were performed at 1.5T (FRC and TLC for eight subjects) and at 3T (TLC for seven subjects). In addition, in vivo ADC measurements at 1.5T with ^{19}F-C_3F_8 (FRC and TLC for eight subjects) and ^{129}Xe (FRC and TLC for six subjects) were performed and compared. Details of sequence, parameter choice, and scan procedures used in this work are included in following sections.

2.3.1 | T_2^* mapping

At 1.5T, ^{19}F T_2^* mapping was performed at lung-inflation levels of TLC and FRC, with the following sequence of breathing maneuvers: (1) Four deep breaths were taken of the gas mixture via a three-way valve from a 25-L Douglas bag to fully saturate the lungs; (2) imaging was then performed under breath-hold apnea at TLC (22 s); (3) the volunteers then exhaled through the three-way valve and continued to breath normally with inhaled gas coming from the Douglas bag; and (4) once the volunteer signaled they were able to commence a second breath-hold, imaging was repeated after exhalation to FRC.

From multiecho SPGR acquisition sequences the signal for each echo time ($S_{n_{echo}}$) was fit voxel-wise according to:

$$S_{n_{echo}} \propto S_1 e^{-\frac{\Delta TE(n_{echo}-1)}{T_2^*}}, \tag{1}$$

where ΔTE is the spacing between echoes, n_{echo} is the echo number and S_1 is the amplitude of the first echo image. The fitting was performed only on pixels with an SNR>10 for the first echo at 1.5T ($\Delta TE = 2.3$ ms) and at 3T ($\Delta TE = 1.5$ ms). This corresponds to at least ≥2.5 noise SD for $n_{echo} = 2$, the recommended SNR threshold for pixel-wise truncation of measurements,[51] for $T_2^* > 1.7$ ms at 1.5T and $T_2^* > 1.1$ ms at 3T. To evaluate the distribution of T_2^* within the lungs, averaged histograms of the T_2^* values from all slices and axial, sagittal, and coronal plots of the maps were produced.

2.3.2 | Apparent diffusion coefficient

The signal after an applied trapezoidal bipolar gradient (S_b) is characterized by:

$$S_b = S_0 e^{-bADC} \tag{2}$$

where S_0 is the signal without diffusion gradients, the *ADC* is the apparent diffusion coefficient, and the *b*-value and the diffusion time (Δ) of the applied pulse are described in the work by Al and Da.[34] For effective lung DWI, the length scale of the confining structure (l_s) of the alveoli must be of the same magnitude as the free diffusion length ($l_d = \sqrt{2D_0\Delta}$) or the gradient dephasing length ($l_g = \left(D_0/\gamma G\right)^{1/3}$), which is the average length that a spin must diffuse to dephase by 2π radians.[52] Figure 1 shows the different length scale regimes in relation to potential DWI conditions typically achieved with

TABLE 1 Imaging parameters for the characterization of different MR parameters

Measurement	TE (ms)	TR (ms)	BW (±kHz)	Matrix (pixels^3)	FOV (cm^3)	FA (°)	Average	Breath-hold (s)
1.5T–^{19}F T_2^*	1.9/4.2/6.6	13	6.94	32 × 26 × 16	40 × 32 × 24	80	4	22
3.0T–^{19}F T_2^*	1.3/2.8/4.3	6.5	11.7	53 × 22 × 16[a]	40 × 33 × 24	45	4	17
1.5T–^{19}F ADC	5.9[b]	10.4	3.01	32 × 26 × 10	40 × 32 × 30	80	4[c]	22
1.5T–^{129}Xe ADC	14.1	17.4	6.94	64 × 52 × 18	40 × 32.5 × 24	3.1	1	16

Abbreviations: BW, bandwidth; FA, flip angle; FOV, field of view; TE, echo time; TR, pulse repetition time.

[a]Elliptical shutter applied (78% acquired in phase encode directions).

[b]Partial Fourier encoding.

[c]Two breath-holds, for double the number of stated averages.

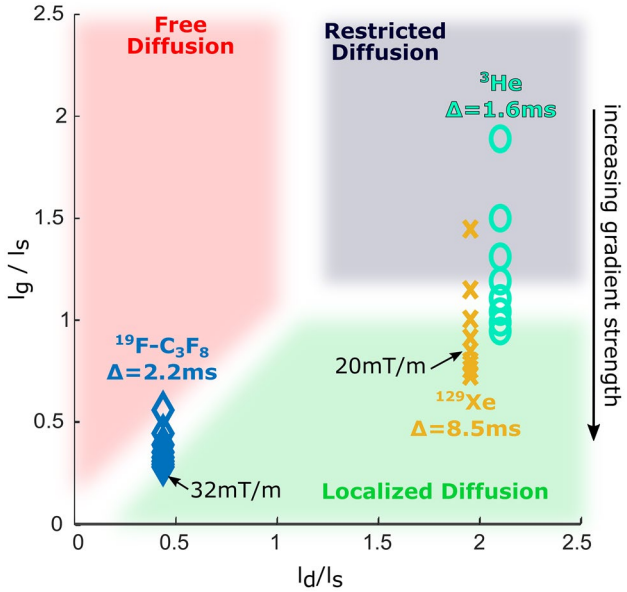

FIGURE 1 Schematic diagram of the three diffusion regimes placing the practical diffusion-weighted imaging conditions with ^{19}F-C_3F_8 (D_0 = 2.7 mm^2/s) in the context of common Δs and diffusion gradient field strengths (plotted from 4 mT/m to 32 mT/m) for the two hyperpolarized gases of ^{129}Xe (D_0 = 14 mm^2/s) and ^{3}He (D_0 = 86 mm^2/s) for a length scale of l_s = 250 μm, with $l_d = \sqrt{2D_0\Delta}$ and $l_g = (D_0/\gamma G)^{1/3}$. The approximate values used for comparison of ^{19}F-C_3F_8 and ^{129}Xe in this study are indicated with arrows

^{129}Xe (D_0 = 14 mm^2/s[9]) and ^{3}He (D_0 = 86 mm^2/s[9]) in air, and C_3F_8 mixed with 79% O_2 (D_0 = 2.7 mm^2/s[26]) for an average alveolar diameter of l_s at approximately 250 μm.[53]

For DWI with ^{129}Xe Δ = 8.5 ms[54] and b = 0.12 s/mm[255] the geometrical parameters derived from models of the acinar airway closely match those obtained with ^{3}He Δ = 1.6 ms, that has been shown to be effective for characterizing lung microstructure[54]; therefore, this diffusion time was used for ^{129}Xe DWI in this study. For C_3F_8 DWI, Δ = 2.2 ms and b = 0.18 s/mm^2 with a gradient echo sequence was used, matching that used previously with C_2F_6.[46] This was expected to put the measurements in the localization regime (see Figure 1), where the ADC signal is dominated by diffusional restriction at the boundaries of the lung alveolar structure.[56] To determine the sensitivity of C_3F_8 ADC to changes in airway microstructural dimensions caused by lung inflation, the ADC was measured at both FRC and TLC and compared with the equivalent ^{129}Xe ADC measurements.

For ^{19}F ADC imaging, the same breathing maneuvers were followed as for T_2^* imaging, except that two additional images were acquired at breath-holds of TLC and FRC (22 s each) obtained sequentially while breathing from the same 25-L Douglas bag. The two images obtained at the same inflation level were averaged together for increased SNR. To perform an independent measurement of the D_0 the same ADC measurement was performed with the Douglas bag on three separate occasions. For ^{129}Xe imaging, a 1-L bag of gas was inhaled from FRC consisting of 400-mL N_2 gas mixed with 600-mL ^{129}Xe.[48] The volunteers then either breathed in room air to TLC or exhaled to FRC prior to imaging during breath-hold (16 s).

All C_3F_8 and ^{129}Xe DW images were thresholded so that only voxels with SNR >15[57] were used in the calculation of ADC. To evaluate the distribution of ADC values at FRC and TLC, histograms of ^{129}Xe and ^{19}F ADC averaged over all slices were plotted for all volunteers. Furthermore, similar to the process carried out in Fichele et al,[42] the ADC gradient in the anteroposterior direction was calculated by first visually identifying the center of the lungs and then plotting the average ADC for each of the slices/pixels relative to the center for all volunteers together.

3 | RESULTS

3.1 | Transverse relaxation—T_2^*

Maps of T_2^* in central axial, coronal, and sagittal slices for volunteer S1 are shown at 1.5T at FRC in Figure 2A, at TLC in Figure 2B, and at 3T at TLC in Figure 2C. The T_2^* values are much lower than those found in phantoms where T_2^* ~T_2~T_1 = 18-22 ms.[20] Also, a clear decrease in T_2^* is observed around the intrapulmonary vessels and the diaphragm, where tissue-air bulk magnetic susceptibility gradients are highest. The recorded mean values for all volunteers are listed in Table 2 along with the *p* value for the paired *t* test comparing changes between the mean T_2^* at FRC and TLC (1.5T) and also between TLC at 1.5T and 3T, which is demonstrated clearly in the histograms of the T_2^* maps shown in Figure 2D.

3.2 | Apparent diffusion coefficient

ADC measurements made in the Douglas bag alone determined a D_0 of 2.54 ± 0.06 mm^2/s for the C_3F_8/O_2 mixture. ADC maps generated from C_3F_8 imaging in volunteer S5 are shown in Figure 3A (at FRC) and Figure 3B (at TLC). The mean ^{19}F-C_3F_8 ADC histograms from all volunteers are shown in Figure 3C.

Because of our chosen rejection criterion of SNR <15 on voxels when mapping ADC, there was a consistent exclusion of areas around the major pulmonary vessels, and in some regions around the diaphragm of volunteers in C_3F_8 imaging. This was caused by the reduced signal from lower T_2^* and partial voluming in these regions, as observed in Figure 1, and also the longer TE required for the ADC sequence. Figure 3D-F shows equivalent maps generated from ^{129}Xe imaging in the same volunteer. The ADC maps in Figure 3

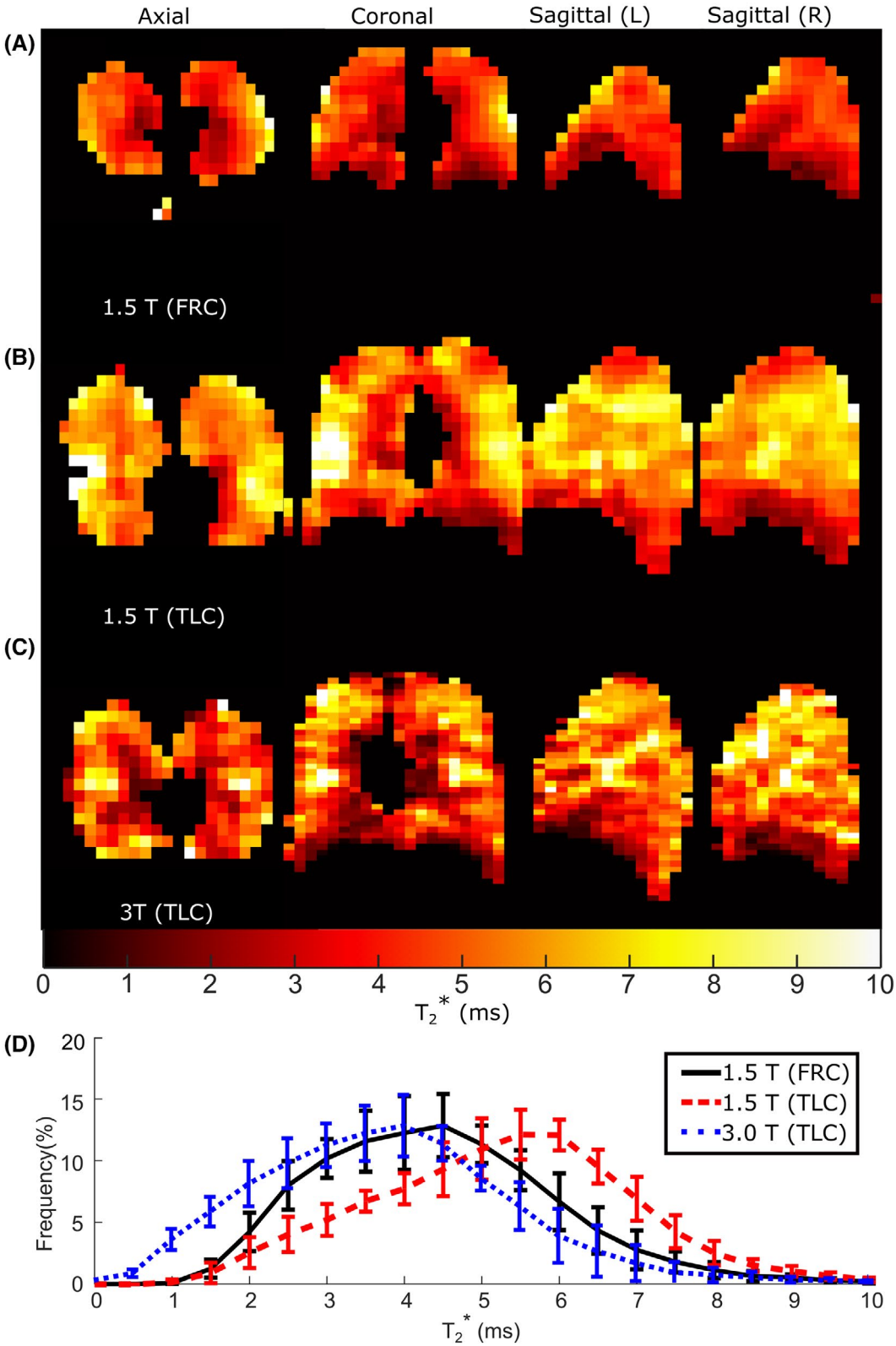

FIGURE 2 T_2^* maps for $^{19}F/C_3F_8$ in central slices for a representative volunteer. A, Functional residual capacity (FRC) and 1.5T. B, Total lung capacity (TLC) and 1.5T. C, TLC and 3T. D, Mean T^* histogram line plots in healthy volunteers with $^{19}F/C_3F_8$: at TLC and 1.5T, at FRC and 1.5T and at TLC and 3T. Bin widths are 0.5 ms and error bars show the standard deviation across all volunteers

show regions of heterogeneous ADC near the heart and to the inferior of the lungs, as well as localized regions of lower than average ADC. Table 2 shows the mean ADC values for all volunteers and the p values for the paired t tests comparing changes between the mean ADC at FRC to TLC for both ^{19}F-C_3F_8 and ^{129}Xe.

TABLE 2 Summary of apparent diffusion coefficient and T_2^* parameter values measured in all volunteers

	^{19}F-$C_3F_8T_2^*$ (ms)			^{19}F-C_3F_8 ADC (mm^2/s) at 1.5T		^{129}Xe ADC (mm^2/s) at 1.5T	
Volunteer	**FRC at 1.5T SNR 23.9 ± 5.0**	**TLC at 1.5T SNR 27.8 ± 8.7**	**TLC at 3T SNR 23.5 ± 7**	**FRC SNR - 25.9 ± 6.3**	**TLC SNR 36.4 ± 6.3**	**FRC SNR 25.2 ± 1.5**	**TLC SNR 23.8 ± 4.6**
S1	4.20 ± 1.56	5.55 ± 1.89	4.63 ± 2.08	1.70 ± 0.34	1.87 ± 0.37	2.23 ± 1.05	3.61 ± 1.19
S2	4.33 ± 1.65	5.22 ± 1.93	3.76 ± 1.47	1.49 ± 0.36	1.71 ± 0.41	2.56 ± 00.74	3.29 ± 0.72
S3	4.48 ± 1.30	5.15 ± 1.39	4.03 ± 1.93	1.70 ± 0.51	1.80 ± 0.54	2.38 ± 1.02	3.20 ± 0.96
S4	4.54 ± 1.54	5.65 ± 1.98	3.45 ± 1.35	1.39 ± 0.39	1.70 ± 0.48	2.32 ± 0.93	3.56 ± 1.17
S5	5.19 ± 1.97	5.52 ± 1.88	3.65 ± 1.57	1.33 ± 0.32	1.73 ± 0.42	2.66 ± 0.98	3.38 ± 0.81
S6	4.53 ± 1.68	5.19 ± 2.02	3.37 ± 1.45	1.81 ± 0.36	1.91 ± 0.38	2.76 ± 1.21	3.23 ± 0.74
S7	4.48 ± 1.57	5.49 ± 1.87	3.59 ± 1.44	1.49 ± 0.33	2.03 ± 0.45	N/A	N/A
S8	4.10 ± 1.52	4.90 ± 1.72	N/A	1.57 ± 0.36	1.85 ± 0.43	N/A	N/A
Total mean	4.48 ± 0.33	5.33 ± 0.26	3.78 ± 0.43	1.56 ± 0.17	1.83 ± 0.11	2.49 ± 0.21	3.38 ± 0.17
paired *t* test	FRC 1.5T → TLC 1.5T $P = .0001$	TLC 1.5T → TLC 3T $P = .0009$		FRC → TLC $P = .0017$		FRC → TLC $P = .0015$	
				Linear regression of ^{19}F-C_3F_8 ADC (slope) mm^2/s per cm + (intercept) mm^2/s		Linear regression of ^{129}Xe ADC (slope) mm^2/s per cm + (intercept) mm^2/s	
				FRC ^{19}F-C_3F_8	TLC ^{19}F-C_3F_8	FRC ^{129}Xe	TLC ^{129}Xe
			Posterior to anterior (inferior half of lungs)	0.0390 + 1.66 $r^2 = 0.980$	N/A - $r^2 < 0.7$	0.0988 + 2.62 $r^2 = 0.859$	0.0310 + 3.50 $r^2 = 0.842$
			Posterior to anterior (superior half of lungs)	0.0308 + 1.50 $r^2 = 0.971$	0.0168 + 1.82 $r^2 = 0.868$	0.0871 + 2.31 $r^2 = 0.893$	0.0326 + 3.30 $r^2 = 0.785$

Notes: The mean and standard deviation of the image SNR across all volunteers is listed with the lung inflation state of the measurements. The linear gradients measured for ADC values in the anterior to posterior direction are provided with the exclusion criterion that the linear regression $r^2 > 0.7$.

Abbreviations: ASC, apparent diffusion coefficient; FRC, functional residual capacity; TLC, total lung capacity; SNR, signal-to-noise ratio.

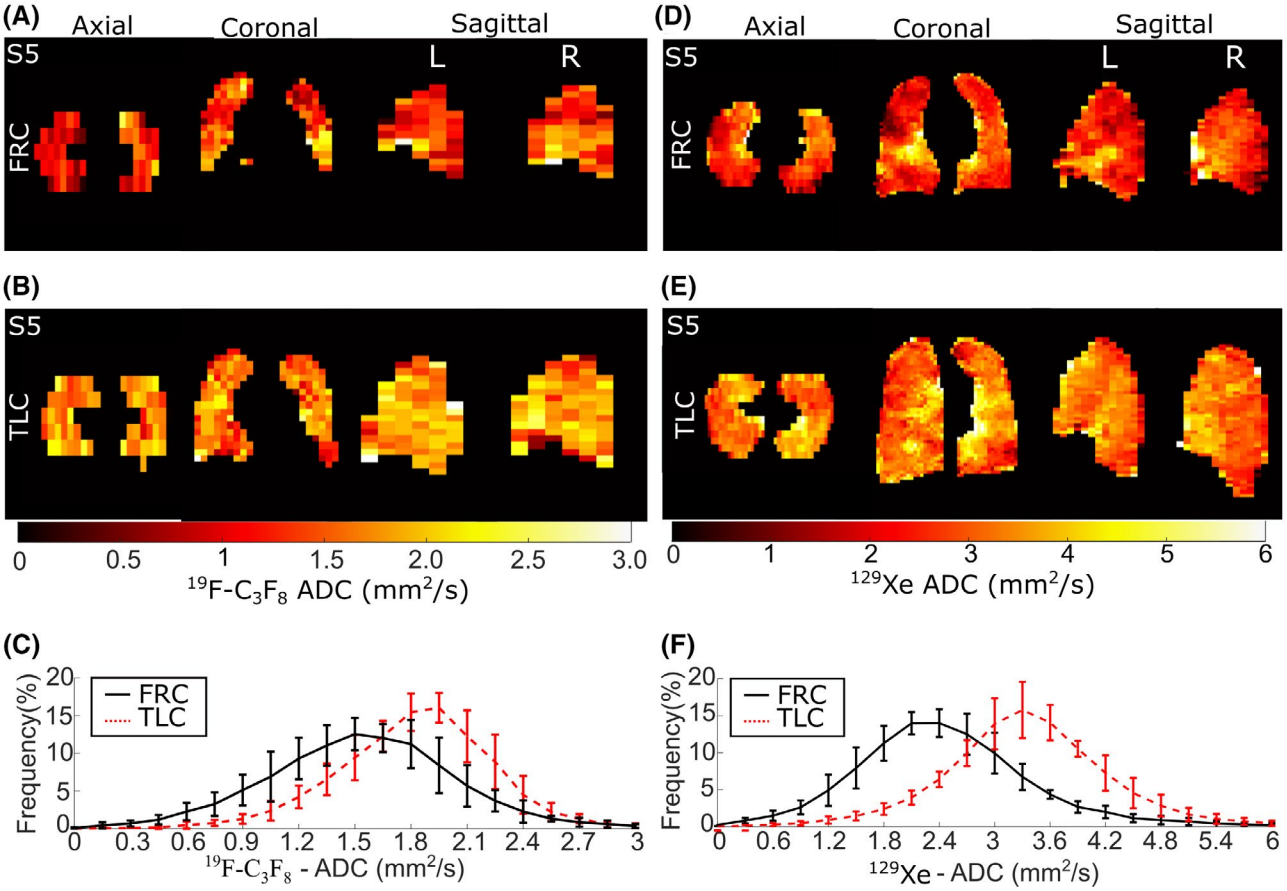

FIGURE 3 Apparent diffusion coefficient (ADC) maps for $^{19}F/C_3F_8$ in central slices for a representative volunteer measured at 1.5T. (A) Functional residual capacity (FRC) and (B) total lung capacity (TLC) with (C) mean ADC histogram line plots in healthy volunteers. Also, similar ADC maps for ^{129}Xe at (D) FRC and (E) TLC are shown, as well as (F) histogram line plots. In histogram plots, error bars show the standard deviation across all volunteers and bin widths are 0.15 mm^2/s and 0.3 mm^2/s, respectively

The results from linear regression of the anteroposterior anatomical gradients in ADC are presented in Table 2. Plots of the linear variation can be viewed in Supporting Information Figure S1.

4 | DISCUSSION

4.1 | T_2^*

The mean T_2^* of C_3F_8 in lungs of volunteers was found to be higher than previously reported (1.5-2.2 ms[23,58]). These previous measurements were performed as global whole lung spectroscopy and the returned T_2^* values are expected to be lower because of the wider B_0 inhomogeneity across the entire lung when compared with an imaging voxel. The variation of T_2^* between volunteers is predicted to be primarily dependent on the normal variations in alveolar dimensions within the population[59] and the susceptibility effects from the inhomogeneity of the tissue interfaces (differences in the bulk magnetic susceptibility[60] at the air–tissue interfaces of alveoli[61]). Therefore, it is expected that microscopic susceptibility differences associated with different disease pathologies may also show changes in T_2^*. Our work indicates that ^{19}F T_2^* mapping at 1.5T is less technically challenging than at 3T because a longer T_2^* is observed at 1.5T, which is consistent with previous results obtained with HP gases.[5,6,31]

4.2 | Apparent diffusion coefficient

For C_3F_8, longer diffusion times are required to match the same length scale as those sensitized in ^3He and ^{129}Xe DWI; achieving these is hindered by the low T_2^* and SNR. Although a spin-echo sequence could potentially be used to mitigate this, ^{19}F- C_3F_8 DWI with a spin-echo–based sequence would result in unfeasible breath-hold times because of specific absorption rate constraints and RF power restrictions on RF-pulse duration and B_1 amplitude. In addition, any further gains in SNR are predicted to be limited because of the transmit homogeneity of the vest RF coil and the longer sequence TR of a spin-echo mandating reduced averaging. In future studies, spin-echo–based sequences could potentially be applied for the benefit of increased diffusion times.

The measured in vivo ADC values are lower than the measured (D_0 = ~2.54 mm^2/s) and previously published (D_0 = ~2.7 mm^2/s[26]) free diffusion coefficients of C_3F_8 mixed with 21% O_2, showing some sensitivity to acinar diffusion restriction. The in vivo healthy volunteer C_3F_8 ADC values are similar to those acquired from excised healthy lungs with C_2F_6 (1.8 mm^2/s[46]). In addition, clear changes in ADC between FRC and TLC were observed, as well as regional differences caused by the gravitational gradient at FRC, but not at TLC. In previous work with ^{3}He, a similar gradient in ADC was observed in the anteroposterior direction,[37,42] that was reduced or not observable at TLC.[39] Furthermore, previously with ^{129}Xe in healthy volunteers, a 22% decrease in the mean ADC was found from the anterior to the posterior of the lungs in healthy volunteers, which was not observed in patients with chronic obstructive pulmonary disease.[38] A decreasing gradient in the superoinferior direction has also been reported,[37,38,42] but was not observed in this study. Two factors may have masked the measurement of this gradient: (1) the gradient depends on the posture of the imaging subject,[42] and (2) regions of the lung next to the heart experience compression, which results in regional changes in ADC that have been observed in HP gas-diffusion imaging.[62]

Based on the observed changes with lung inflation, there is a strong indication from this work that the DWI parameters used here for in vivo ^{19}F-C_3F_8 ADC mapping will be able to detect changes in lung microstructure in different pathologies where changes are larger, such as in emphysema where the measured ^{3}He ADC can increase by a factor of two to three when compared with healthy lungs,[63] or in idiopathic pulmonary fibrosis where the ^{3}He ADC can increase by a factor of three to five in regions of fibrotic tissue.[36] Previous attempts at in vivo ADC measurements of C_3F_8 in experiments with a single volunteer resulted in a maximum image SNR of approximately 15,[58,64] which is below the threshold set here for inclusion of voxels in the ADC calculation. In addition, these previous studies used shorter diffusion times (Δ = 1 ms) and smaller b-values (0.0959 s/mm^2 [58] and 0.0133 s/cm^2,[64] which places those measurements in the free diffusion regime. The reported ADC values in some regions were ≥6 mm^2/s, which far exceeds the free diffusion coefficient and may have been a result of the low SNR and the weak b-values used in that work. In future work, ensuring that the gas mixture concentration in the lungs reaches full saturation of 79% perfluoropropane per 21% O_2 is necessary because the partial pressure strongly influences the free diffusion coefficient (approximately D_0 = ~2.3-7.7 mm^2/s for 100%-0% partial pressure with O_2).

5 | CONCLUSIONS

By utilizing improvements in receiver design, optimized imaging parameters, and breathing maneuvers, three-dimensional in vivo ADC mapping with C_3F_8 in the human lungs was found to be feasible with a greater resolution than previously attempted. Thus, for the first time, systematic in vivo mapping of ADC at 1.5T and T_2^* at the two clinically relevant MRI field strengths (3T and 1.5T) is presented for C_3F_8 in the lungs of healthy volunteers, indicating sensitivity to change in acinar airways dimensions. These results show promise for future studies in lung diseases that exhibit microstructural airway changes.

ACKNOWLEDGMENTS

This work was supported by the National Institute for Health Research (NIHR-RP-R3-12-027), the Medical Research Council (MR/M008894/1), the National Sciences and Engineering Research Council of Canada (NSERC), an investigator-led research grant from GE Healthcare, and by LIFT MRC project MR/N018915/1, which helped fund the 3T birdcage coil.

Paul J.C Hughes is funded by a research grant from GlaxoSmithKline (BIDS3000032592). Thanks to Rolf F. Schulte (GE Global Research, Munich, Germany) for use of the Fidall sequence programming for 1.5T T_2^* mapping. Thanks to Felix Horn for useful early discussion and training in C_3F_8 delivery. Views expressed in this publication are those of the authors and not necessarily those of the National Health Service, the National Institute for Health Research, or the UK Department of Health.

CONFLICT OF INTEREST

Employee relationship to GE Healthcare, Inc which partially funded the work.

ORCID

Adam Maunder https://orcid.org/0000-0002-1161-8741
Ho-Fung Chan https://orcid.org/0000-0002-5382-2097
Paul J. C. Hughes https://orcid.org/0000-0002-7979-5840
Guillhem Collier https://orcid.org/0000-0002-1874-4775
Graham Norquay https://orcid.org/0000-0002-4108-9035
Peter Thelwall https://orcid.org/0000-0003-1795-6394
Madhwesha Rao https://orcid.org/0000-0002-4109-4176
Jim M. Wild https://orcid.org/0000-0002-7246-8660

REFERENCES

1. Pavlova OS, Anisimov NV, Gervits LL, et al. 19F MRI of human lungs at 0.5 Tesla using octafluorocyclobutane. *Magn Reson Med*. 2020;84:2117-2123.
2. Altes TA, Powers PL, Knight-Scott J, et al. Hyperpolarized 3He MR lung ventilation imaging in asthmatics: Preliminary findings. *J Magn Reson Imaging*. 2001;13:378-384.
3. Kauczor H-U, Ebert M, Kreitner K-F, et al. Imaging of the lungs using 3He MRI: Preliminary clinical experience in 18 patients with and without lung disease. *J Magn Reson Imaging*. 1997;7:538-543.

4. Kauczor H, Hanke A, Beek V, Edwin JR. Assessment of lung ventilation by MR imaging: Current status and future perspectives. *Eur Radiol*. 2002;12:1962-1970.
5. Ajraoui S, Parra-Robles J, Marshall H, Deppe MH, Clemence M, Wild JM. Acquisition of 3He ventilation images, ADC, T2* and B1 maps in a single scan with compressed sensing. *NMR Biomed*. 2012;25:44-51.
6. Xu X, Norquay G, Parnell SR, et al. Hyperpolarized 129Xe gas lung MRI?SNR and T2* comparisons at 1.5 T and 3 T. *Magn Reson Med*. 2012;68:1900-1904.
7. Chen XJ, Möller HE, Chawla MS, et al. Spatially resolved measurements of hyperpolarized gas properties in the lung in vivo. Part II: T*(2). *Magn Reson Med*. 1999;42:729-737.
8. Möller HE, Hedlund LW, Chen XJ, et al. Measurements of hyperpolarized gas properties in the lung. Part III: (3)He T(1). *Magn Reson Med*. 2001;45:421-430.
9. Kruger SJ, Nagle SK, Couch MJ, Ohno Y, Albert M, Fain SB. Functional imaging of the lungs with gas agents. *J Magn Reson Imaging*. 2016;43:295-315.
10. Chen XJ, Möller HE, Chawla MS, et al. Spatially resolved measurements of hyperpolarized gas properties in the lung in vivo. Part I: Diffusion coefficient. *Magn Reson Med*. 1999;42:721-728.
11. Diaz S, Casselbrant I, Piitulainen E, et al. Hyperpolarized 3He apparent diffusion coefficient MRI of the lung: Reproducibility and volume dependency in healthy volunteers and patients with emphysema. *J Magn Reson Imaging*. 2008;27:763-770.
12. Chan H, Stewart NJ, Parra-Robles J, Collier GJ, Wild JM. Whole lung morphometry with 3D multiple b-value hyperpolarized gas MRI and compressed sensing. *Magn Reson Med*. 2017;77:1916-1925.
13. Ouriadov A, Farag A, Kirby M, McCormack DG, Parraga G, Santyr GE. Lung morphometry using hyperpolarized (129) Xe apparent diffusion coefficient anisotropy in chronic obstructive pulmonary disease. *Magn Reson Med*. 2013;70:1699-1706.
14. Wild JM, Teh K, Woodhouse N, et al. Steady-state free precession with hyperpolarized 3He: Experiments and theory. *J Magn Reson*. 2006;183:13-24.
15. Deppe MH, Wild JM. Variable flip angle schedules in bSSFP imaging of hyperpolarized noble gases. *Magn Reson Med*. 2012;67:1656-1664.
16. Stewart NJ, Norquay G, Griffiths PD, Wild JM. Feasibility of human lung ventilation imaging using highly polarized naturally abundant xenon and optimized three-dimensional steady-state free precession. *Magn Reson Med*. 2015;74:346-352.
17. Stewart NJ, Chan H, Hughes PJC, et al. Comparison of 3He and 129Xe MRI for evaluation of lung microstructure and ventilation at 1.5T. *J Magn Reson Imaging*. 2018;48:632-642
18. Neal MA, Pippard BJ, Hollingsworth KG, et al. Optimized and accelerated 19F-MRI of inhaled perfluoropropane to assess regional pulmonary ventilation. *Magn Reson Med*. 2019;82:1301-1311.
19. Couch MJ, Ball IK, Li T, et al. Pulmonary ultrashort echo time 19F MR imaging with inhaled fluorinated gas mixtures in healthy volunteers: Feasibility. *Radiology*. 2013;269:903-909.
20. Maunder A, Rao M, Robb F, Wild JM. Optimization of steady-state free precession MRI for lung ventilation imaging with 19F C3F8 at 1.5T and 3T. *Magn Reson Med*. 2019;81:1130-1142.
21. Ebner B, Behm P, Jacoby C, et al. Early assessment of pulmonary inflammation by 19F MRI in vivo. *Circ Cardiovasc Imaging*. 2010;3:202-210.
22. Obert AJ, Gutberlet M, Kern AL, et al. 1H-guided reconstruction of 19F gas MRI in COPD patients. *Magn Reson Med*. 2020;84:1336-1346.
23. Neal MA, Pippard BJ, Simpson AJ, Thelwall PE. Dynamic susceptibility contrast 19F-MRI of inhaled perfluoropropane: A novel approach to combined pulmonary ventilation and perfusion imaging. *Magn Reson Med*. 2020;83:452-461.
24. Weiskopf N, Suckling J, Williams G, et al. Quantitative multi-parameter mapping of R1, PD*, MT, and R2* at 3T: A multi-center validation. *Front Neurosci*. 2013;7:1-11.
25. Gai ND, Malayeri AA, Bluemke DA. Three-dimensional T1 and T2* mapping of human lung parenchyma using interleaved saturation recovery with dual echo ultrashort echo time imaging (ITSR-DUTE). *J Magn Reson Imaging*. 2017;45:1097-1104.
26. Chang YV, Conradi MS. Relaxation and diffusion of perfluorocarbon gas mixtures with oxygen for lung MRI. *J Magn Reson*. 2006;181:191-198.
27. Adolphi NL, Kuethe DO. Quantitative mapping of ventilation-perfusion ratios in lungs by 19F MR imaging of T1 of inert fluorinated gases. *Magn Reson Med*. 2008;59:739-746.
28. Mugler JP, Altes TA. Hyperpolarized 129Xe MRI of the human lung. *J Magn Reson Imaging*. 2013;37:313-331.
29. Saam B, Happer W, Middleton H. Nuclear relaxation of 3He in the presence of O2. *Phys Rev A*. 1995;52:862-865.
30. Deppe MH, Parra-Robles J, Ajraoui S, et al. Susceptibility effects in hyperpolarized 3He lung MRI at 1.5T and 3T. *J Magn Reson Imaging*. 2009;30:418-423.
31. Komlosi P, Altes TA, Qing K, et al. Signal-to-noise ratio, T2, and T2* for hyperpolarized helium-3 MRI of the human lung at three magnetic field strengths. *Magn Reson Med*. 2017;78:1458-1463.
32. Thomen RP, Quirk JD, Roach D, et al. Direct comparison of 129 xe diffusion measurements with quantitative histology in human lungs. *Magn Reson Med*. 2017;77:265-272.
33. Yablonskiy DA, Sukstanskii AL, Woods JC, et al. Quantification of lung microstructure with hyperpolarized 3He diffusion MRI. *J Appl Physiol (1985)*. 2009;107:1258-1265.
34. Al S, Da Y. Lung morphometry with hyperpolarized 129Xe: Theoretical background. *Magn Reson Med*. 2011;67:856-866.
35. Mammarappallil JG, Rankine L, Wild JM, Driehuys B. New developments in imaging idiopathic pulmonary fibrosis with hyperpolarized xenon magnetic resonance imaging. *J Thorac Imaging*. 2019;34:136-150.
36. Chan H, Weatherley ND, Johns CS, et al. Airway microstructure in idiopathic pulmonary fibrosis: Assessment at hyperpolarized ^{3}He diffusion-weighted MRI. *Radiology*. 2019;291:223-229.
37. Evans A, McCormack D, Ouriadov A, Etemad-Rezai R, Santyr G, Parraga G. Anatomical distribution of 3He apparent diffusion coefficients in severe chronic obstructive pulmonary disease. *J Magn Reson Imaging*. 2007;26:1537-1547.
38. Kaushik SS, Cleveland ZI, Cofer GP, et al. Diffusion-weighted hyperpolarized 129Xe MRI in healthy volunteers and subjects with chronic obstructive pulmonary disease. *Magn Reson Med*. 2011;65:1154-1165.
39. Halaweish AF, Hoffman EA, Thedens DR, Fuld MK, Sieren JP, van Beek EJR. Effect of lung inflation level on hyperpolarized ^{3}He apparent diffusion coefficient measurements in never-smokers. *Radiology*. 2013;268:572-580.
40. Hajari AJ, Yablonskiy DA, Sukstanskii AL, Quirk JD, Conradi MS, Woods JC. Morphometric changes in the human pulmonary acinus during inflation. *J Appl Physiol*. 2012;112:937-943.

41. Quirk JD, Sukstanskii AL, Woods JC, et al. Experimental evidence of age-related adaptive changes in human acinar airways. *J Appl Physiol*. 2016;120:159-165.
42. Fichele S, Woodhouse N, Swift AJ, et al. MRI of helium-3 gas in healthy lungs: Posture related variations of alveolar size. *J Magn Reson Imaging*. 2004;20:331-335.
43. Carrero-González L, Kaulisch T, Stiller D. In vivo diffusion-weighted MRI using perfluorinated gases: ADC comparison between healthy and elastase-treated rat lungs. *Magn Reson Med*. 2013;70:1761-1764.
44. Ruiz-Cabello J, Pérez-Sánchez JM, Pérez de Alejo R, et al. Diffusion-weighted 19F-MRI of lung periphery: Influence of pressure and air–SF6 composition on apparent diffusion coefficients. *Respir Physiol Neurobiol*. 2005;148:43-56.
45. Pérez-Sánchez JM, Pérez de Alejo R, Rodríguez I, Cortijo M, Peces-Barba G, Ruiz-Cabello J. In vivo diffusion weighted ^{19}F MRI using SF_6. *Magn Reson Med*. 2005;54:460-463.
46. Jacob RE, Chang YV, Choong CK, et al. ^{19}F MR imaging of ventilation and diffusion in excised lungs. *Magn Reson Med*. 2005;54:577-585.
47. Conradi M, Saam B, Yablonskiy D, Woods J. Hyperpolarized ^{3}He and perfluorocarbon gas diffusion MRI of lungs. *Prog Nucl Magn Reson Spectrosc*. 2006;48:63-83.
48. Norquay G, Collier GJ, Rao M, Stewart NJ, Wild JM. 129Xe-rb spin-exchange optical pumping with high photon efficiency. *Phys Rev Lett*. 2018;121:153201.
49. Maunder A, Robb F, Rao M, Wild J. Application of asymmetric mode ladder resonators for improved efficiency of individual elements in transceive arrays. *Proc Intl Soc Mag Reson; Honolulu, Hawai'i, USA*. 2017;25:1052.
50. Maunder A, Rao M, Robb F, Wild JM. An 8-element Tx/Rx array utilizing MEMS detuning combined with 6 Rx loops for ^{19}F and ^{1}H lung imaging at 1.5T. *Magn Reson Med*. 2020;84:2262-2277.
51. Sandino CM, Kellman P, Arai AE, Hansen MS, Xue H. Myocardial T_2* mapping: Influence of noise on accuracy and precision. *J Cardiovasc Magn Reson*. 2015;17:7.
52. Parra-Robles J, Ajraoui S, Deppe MH, Parnell SR, Wild JM. Experimental investigation and numerical simulation of 3He gas diffusion in simple geometries: Implications for analytical models of 3He MR lung morphometry. *J Magn Reson*. 2010;204:228-238.
53. Haefeli-Bleuer B, Weibel ER. Morphometry of the human pulmonary acinus. *Anat Rec*. 1988;220:401-414.
54. Parra-Robles J, Wild JM. The influence of lung airways branching structure and diffusion time on measurements and models of short-range 3He gas MR diffusion. *J Magn Reson*. 2012;225:102-113.
55. Chan H, Stewart NJ, Norquay G, Collier GJ, Wild JM. 3D diffusion-weighted 129Xe MRI for whole lung morphometry. *Magn Reson Med*. 2018;79:2986-2995.
56. Moutal N, Demberg K, Grebenkov D, Kuder TA. Localization regime in diffusion NMR: Theory and experiments. *J Magn Reson*. 2019;305:162-174.
57. O'Halloran RL, Holmes JH, Altes TA, Salerno M, Fain SB. The effects of SNR on ADC measurements in diffusion-weighted hyperpolarized he-3 MRI. *J Magn Reson*. 2007;185:42-49.
58. Couch MJ, Ball IK, Li T, et al. Inert fluorinated gas MRI: A new pulmonary imaging modality. *NMR Biomed*. 2014;27:1525-1534.
59. Ochs M, Nyengaard JR, Jung A, et al. The number of alveoli in the human lung. *Am J Respir Crit Care Med*. 2004;169:120-124.
60. Yablonskiy DA, Haacke EM. Theory of NMR signal behavior in magnetically inhomogeneous tissues: The static dephasing regime. *Magn Reson Med*. 1994;32:749-763.
61. Durney CH, Bertolina J, Ailion DC, et al. Calculation and interpretation of inhomogeneous line broadening in models of lungs and other heterogeneous structures. *J Magn Reson*. 1989;85:554-570.
62. Albert R, Hubmayr R. The prone position eliminates compression of the lungs by the heart. *Am J Respir Crit Care Med*. 2000;161:1660-1665.
63. Parraga G, Ouriadov A, Evans A, et al. Hyperpolarized 3He ventilation defects and apparent diffusion coefficients in chronic obstructive pulmonary disease: Preliminary results at 3.0 tesla. *Invest Radiol*. 2007;42:384-391.
64. Ball IK, Couch MJ, Li T, et al. 19F apparent diffusion coefficient MRI of inert fluorinated gases in human lungs. *Proc Intl Soc Mag Reson Med; Salt Lake City, Utah, USA*. 2013;21:1483.

SUPPORTING INFORMATION

Additional supporting information may be found online in the Supporting Information section.

FIGURE S1 The mean ADC in slices moving in the anteroposterior (left) or superior-inferior (right) directions, separated for either the superior or inferior halves or the anterior or posterior halves of the lungs, respectively. The variation in ADC is plotted for $^{19}F/C_3F_8$ at A, FRC and B, TLC, as well as for ^{129}Xe at C, FRC and D, TLC

How to cite this article: Maunder A, Chan H, Hughes PJC, et al. MR properties of ^{19}F C_3F_8 gas in the lungs of healthy volunteers: T_2^* and apparent diffusion coefficient at 1.5T and T_2^* at 3T. *Magn Reson Med*. 2021;85:1561–1570. https://doi.org/10.1002/mrm.28511